2020 IEEE/RSJ International Conference on Intelligent Robots and Systems (IROS)
October 25-29, 2020, Las Vegas, NV, USA (Virtual)

Objective Functions of Principal Contact Estimation from Motion Based on the Geometrical Singular Condition

Seiya Ishikawa[1], Shouhei Shirafuji[2], and Jun Ota[2]

Abstract— **In this paper, we propose objective functions to estimate the principal contact between a unknown manipulated target object and its unknown surroundings from the motion of the object. We derived the objective functions based on the fact that contact involves a pair of geometrical primitives (a point of vertex, a line of edge, and a plane of face) for the singular condition of the calculation for their intersection or their spanned space from the point of view of geometrical algebra. The minimization of the proposed objective functions, which are differential quadratic forms of the Kronecker product of geometrical parameters, efficiently provided us the contact geometries that constrained the object movements. Additionally, the proposed objective functions are fundamentals for identifying contact during compliant manipulation, and we showed that the objective functions provide a clue for contact identification via experiments.**

I. INTRODUCTION

Proper use of contact between an object and its surroundings helps to accomplish many types of manipulation tasks. For example, in industrial assembly, we can assemble a mechanical part by moving it along with the assembling target part via contact and sensing the change in contact precisely. In the case of loading and unloading packages in warehouses, sliding a loading package on another package saves power compared to lifting it. The above types of manipulation tasks that make use of the environment are essential for realizing dexterous robotic manipulation and compliant motion tasks [1].

We need to determine how the manipulation target object and its surroundings contact each other to achieve compliant motion without applying unnecessary force. Many studies on compliant motion describe contact between an object and the environment by contact formation (CF) [2]. CF is a concept used to denote the contact between two polyhedrons and contains information about which surface elements (i.e., faces, edges, or vertices) of an object contact with the surface elements of the other object. Estimation of CF from the force and position during robotic manipulation or a demonstration for teaching a robot is the key technology for realizing compliant motion tasks. On approach for estimating the CF is generating the CF graph first and calculating the possible sensor values [3] for each CF depending on the constraints caused by the contact. Machine learning techniques have also been used to estimate CF. The CF can be estimated by comparing possible sensor values with the actual sensor value at each CF. Although many studies have used both the force and position sensing to estimate the CF [4]–[9], some studies have relied only on force measurements [10] or position measurements [11] for estimating the CF.

Most estimation methods require data on the shape of the object and the environment in advance. However, it is difficult to know the shape of an object and the environment for many manipulation situations. To cope with unknown shape objects, Mimura et al. [12] and Mouri et al. [13] used the active sensing of force to estimate the contact types and geometrical information of the contact. Mouri et al. [14] also proposed an estimation method with active sensing of the position. Their method estimated the contact types, which were classified by Mason [15], and geometrical information about where the line and point of contact were. They assumed that the contact location does not move with respect to the environment. Thus, we cannot apply their method to the more general case of compliant motion with sliding between an object and its environment.

An ideal contact estimation of general compliant manipulation requires a method to identify the contact types and the contact location for the general compliant motion, such as the object's motion along with another object, from its motion, force, or both, even if we have no idea about the geometry of the object or its surroundings. This paper presents our first attempt to estimate the contact between an unknown shaped object and the environment from the position and orientation of the object during compliant motion. Here, we only focus on the motion of the object and not on the forces applied to the object to clarify the theoretical limitations to estimate the contact only from the motion. Using the premise that the object and environment are both convex polyhedrons, we estimated the principal contact (PC) of a CF [16], [17] (we explain the details of the assumptions and the PCs in the next section) and the geometric information about the contact. As a basis for the contact estimation between an unknown object and its unknown environment, we propose objective functions based on the constraints on the motion for each PC. Here, we describe the objective functions as a quadratic form of the Kronecker product of geometric parameters, and we could efficiently estimate the contact geometries by minimizing these differentiable functions. Additionally, we show that we can reduce the possible contact types by comparing the results of optimization that use the objective functions via experiments.

The remainder of this paper is organized as follows. In Section II, we give further explanation about the problem.

*This work was supported by JSPS KAKENHI Grant Number 16H06682.

[1]The Department of Precision Engineering, School of Engineering, The University of Tokyo, Tokyo, Japan, [2]Shouhei Shirafuji and Jun Ota are with Research into Artifacts Center, Center for Engineering, School of Engineering, The University of Tokyo, Tokyo 113-8656, Japan ishikawa@race.t.u-tokyo.ac.jp

In Section III, we describe the proposed objective functions to estimate the type of contact. In Section IV, we describe the validation of the proposed functions via experiments. Then, we present the conclusions in Section V.

II. Problem Statement

We propose a method to estimate the contact between a manipulation target object and its surroundings from the measured motion of the object. We assumed that the object and the environment are composed of polyhedrons. Xiao [16] represented the contact between polyhedrons by PCs, and he defined four kinds of PCs, face–face (f–f), face–edge or edge–face (f–e or e–f), face–vertex or vertex–face (f–v or v–f), and edge–edge–cross (e–e–c), excluding some non-realistic PCs, as shown in Fig. 1. We also used a representation of the contacts and denoted the object geometry first in the PC, e.g., e–f for the contact between the object edge and the environmental face. A CF consists of PCs between the target object and other objects. We assumed a single PC for a CF in this study for simplification, but we will discuss the extension of a CF with a single PC to general CF cases in the final section below.

In this paper, we represent the geometry of a face, edge, and vertex using the homogeneous representation of a plane, line, and point in Grassmann–Cayley algebra [18], respectively. First, a plane represented by the homogeneous coordinates is given by

$$\boldsymbol{\Pi} = \begin{bmatrix} \boldsymbol{n} \\ h \end{bmatrix}. \tag{1}$$

If $\|\boldsymbol{n}\| = 1$, $\boldsymbol{n}$ is the normal vector of the plane, and h is the length of the perpendicular line to the plane. We represent a line using the homogeneous representation as

$$\boldsymbol{L} = \begin{bmatrix} \boldsymbol{d} \\ \boldsymbol{q} \times \boldsymbol{d} \end{bmatrix} = \begin{bmatrix} \boldsymbol{d} \\ \boldsymbol{m} \end{bmatrix}. \tag{2}$$

If $\|\boldsymbol{d}\| = 1$, $\boldsymbol{d}$ is the direction of the line, and $\boldsymbol{q}$ is a point on the line. Finally, a point is given by

$$\boldsymbol{P} = \begin{bmatrix} \boldsymbol{q} \\ \alpha \end{bmatrix}. \tag{3}$$

If $\alpha = 1$, $\boldsymbol{q}$ is an usual point in a three dimensional(3D) space.

Here, we define the object frame and the spatial frame. The object frame is the coordinate system frame fixed to anywhere on the manipulation target object, and the spatial frame is the coordinate system frame fixed to the world. We describe the above geometries using a superscript to clarify which frame we are representing, e.g., $\boldsymbol{L}^{\mathrm{b}}$ is a line in the object frame and $\boldsymbol{L}^{\mathrm{s}}$ is a line in the spatial frame. Additionally, we add a subscript to the geometry notation, such as $\boldsymbol{L}_{\mathrm{o}}$ and $\boldsymbol{L}_{\mathrm{e}}$, to distinguish the contact on the object and environment, respectively. Thus, the contact geometry of the environment ovserved from the spatial frame and the contact geometry of the object observed from the object frame do not change as the object moves, e.g., $\boldsymbol{L}_{\mathrm{o}}^{\mathrm{b}}$ and $\boldsymbol{L}_{\mathrm{e}}^{\mathrm{s}}$. In the latter sections, the proposed optimization method is used to find the contact geometries; environmental contact in the spatial frame and the object contact in the object frame, which keeps contact during the measured rigid body motion of the object. For k measurements, we describe the motion of the rigid body using $\boldsymbol{R}_i$ and $\boldsymbol{p}_i$, which are the rotational matrix and the position where we observe the spatial frame from the object frame, respectively.

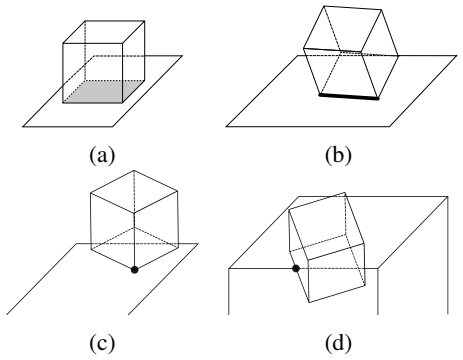

Fig. 1: Four kinds of contact primitives; (a) f–f, (b) f–e or e–f (c) f–v or v–f, and (d) e–e–c.

Our approach for estimating PCs from only the object motion in this study has some limitations, and we included some assumptions as follows. If the PC transits to another PC instantly compared to the measurement of movement, it is difficult to estimate the contact. Thus, we assume a contact keeps that contact state for sufficient time compared to the sampling time. Additionally, some specified motion makes it theoretically impossible to identify its PC. For example, if an object with an e–f contact translates along the environmental plane without rotation, the constraint on the motion is the same as with a f–f contact. This kind of motion is the singular case of the object's movement under the contact constraint. Even in the singular case, there are cases in which we can estimate the PC by classifying the singular cases and measuring the force applied to the object. However, those cases were beyond the scope of this study, and we do not discuss the singular motion in this paper.

III. Contact Estimation

We estimated the contact type represented by contact primitives between the manipulation target object and its surroundings using the geometrical constraint. For example, in an e–f contact, the line of the object edge must remain on the plane of the environmental surface. The geometric condition in which a line is on a plane is the singular condition in the calculation for obtaining the intersection between the line and the plane in 3D space from the viewpoint of the geometrical calculation [19]. By optimizing the location of the edge line in the object coordinate frame and the plane in the spatial coordinate frame to close the singular condition, we can confirm the contact is e–f contact in the above case. Below, we show the objective functions for every case of contact, f–f, e–f, f–e, v–f, f–v, e–e, from the point of view of singularity in the geometrical calculation.

A. f–f contact estimation

In f–f contact, the object face and the environmental face remain in contact with each other during object movement. Usually, two planes intersect each other, and the intersection is a line. By the geometrical calculation using a meet and join operation and dual representation of the geometry in Grassmann–Cayley algebra (see details in ref. [19]), the intersection of two planes on the object and the environment is given by

$$\boldsymbol{L}^{\mathrm{b}} = \begin{bmatrix} h_{\mathrm{e}}^{\mathrm{b}}\boldsymbol{n}_{\mathrm{o}}^{\mathrm{b}} - h_{\mathrm{o}}^{\mathrm{b}}\boldsymbol{n}_{\mathrm{e}}^{\mathrm{b}} \\ \boldsymbol{n}_{\mathrm{o}}^{\mathrm{b}} \times \boldsymbol{n}_{\mathrm{e}}^{\mathrm{b}} \end{bmatrix}. \tag{4}$$

The condition in which the two planes are concurrent is the singular condition of Eq. (4)., i.e., $\boldsymbol{L}^{\mathrm{b}}$ in Eq. (4) becomes a zero vector. Even after taking into account the measurement noise, the norm of the vector must be close to zero if the given planes are correct. Thus, for k measurements, we can find the planes $\boldsymbol{\Pi}_{\mathrm{o}}^{\mathrm{b}}$ and $\boldsymbol{\Pi}_{\mathrm{e}}^{\mathrm{s}}$ by minimizing the following:

$$\begin{aligned} F_{\mathrm{ff}} = \sum_{i=1}^{k} \Big(& \left\| ((\boldsymbol{R}_i \boldsymbol{n}_{\mathrm{e}}^{\mathrm{s}}) \cdot \boldsymbol{p}_i + h_{\mathrm{e}}^{\mathrm{s}})\, \boldsymbol{n}_{\mathrm{o}}^{\mathrm{b}} - h_{\mathrm{o}}^{\mathrm{b}}\, (\boldsymbol{R}_i \boldsymbol{n}_{\mathrm{e}}^{\mathrm{s}}) \right\|^2 \\ & + \left\| \boldsymbol{n}_{\mathrm{o}}^{\mathrm{b}} \times (\boldsymbol{R}_i \boldsymbol{n}_{\mathrm{e}}^{\mathrm{s}}) \right\|^2 \Big). \end{aligned} \tag{5}$$

The summations in Eq. (5) contain the measured values of $\boldsymbol{R}_i$ and $\boldsymbol{p}_i$ through the cross and inner products. Regarding the computational cost for the iterative calculation during the optimization, target variables $\boldsymbol{\Pi}_{\mathrm{o}}^{\mathrm{b}}$ and $\boldsymbol{\Pi}_{\mathrm{e}}^{\mathrm{s}}$ are better removed from the summation. We transformed Eq. (5) as follows:

$$\begin{aligned} F_{\mathrm{ff}} = & \left(\boldsymbol{\Pi}_{\mathrm{o}}^{\mathrm{b}} \otimes \boldsymbol{\Pi}_{\mathrm{e}}^{\mathrm{s}}\right)^{\mathrm{T}} \left(\sum_{i=1}^{k} \boldsymbol{A}_{\mathrm{ff}i}^{\mathrm{T}} \boldsymbol{A}_{\mathrm{ff}i} \right) \left(\boldsymbol{\Pi}_{\mathrm{o}}^{\mathrm{b}} \otimes \boldsymbol{\Pi}_{\mathrm{e}}^{\mathrm{s}}\right) \\ & + \left(\boldsymbol{n}_{\mathrm{o}}^{\mathrm{b}} \otimes \boldsymbol{n}_{\mathrm{e}}^{\mathrm{s}}\right)^{\mathrm{T}} \left(\sum_{i=1}^{k} \boldsymbol{B}_i^{\mathrm{T}} \boldsymbol{B}_i \right) \left(\boldsymbol{n}_{\mathrm{o}}^{\mathrm{b}} \otimes \boldsymbol{n}_{\mathrm{e}}^{\mathrm{s}}\right), \end{aligned} \tag{6}$$

where

$$\boldsymbol{A}_{\mathrm{ff}i} = \begin{bmatrix} \boldsymbol{p}_i^{\mathrm{sbT}} & 1 & \boldsymbol{0}^{\mathrm{T}} & 0 & \boldsymbol{0}^{\mathrm{T}} & 0 & & 0 \\ \boldsymbol{0}^{\mathrm{T}} & 0 & \boldsymbol{p}_i^{\mathrm{sbT}} & 1 & \boldsymbol{0}^{\mathrm{T}} & 0 & -\boldsymbol{R}_i & 0 \\ \boldsymbol{0}^{\mathrm{T}} & 0 & \boldsymbol{0}^{\mathrm{T}} & 0 & \boldsymbol{p}_i^{\mathrm{sbT}} & 1 & & 0 \end{bmatrix} \tag{7}$$

and

$$\boldsymbol{B}_{\mathrm{ff}i} = \begin{bmatrix} \boldsymbol{0}^{\mathrm{T}} & \boldsymbol{r}_{3i}^{\mathrm{T}} & -\boldsymbol{r}_{2i}^{\mathrm{T}} \\ -\boldsymbol{r}_{3i}^{\mathrm{T}} & \boldsymbol{0}^{\mathrm{T}} & \boldsymbol{r}_{1i}^{\mathrm{T}} \\ \boldsymbol{r}_{2i}^{\mathrm{T}} & -\boldsymbol{r}_{1i}^{\mathrm{T}} & \boldsymbol{0}^{\mathrm{T}} \end{bmatrix}. \tag{8}$$

In the above matrices, $\boldsymbol{p}_i^{\mathrm{sb}} = -\boldsymbol{R}_i^{\mathrm{T}} \boldsymbol{p}_i$, and $\boldsymbol{r}_1$, $\boldsymbol{r}_2$, and $\boldsymbol{r}_3$ are the first, second, and third row of $\boldsymbol{R}$ transformed into a column vector, respectively.

If the object moves under the constraint of f–f contact, Eq. (6) has a small value. However, the case of f–f contact is exceptional compared to other contact cases in which $h_{\mathrm{o}}^{\mathrm{b}}$ and $h_{\mathrm{e}}^{\mathrm{s}}$ in $\boldsymbol{\Pi}_{\mathrm{o}}^{\mathrm{b}}$ and $\boldsymbol{\Pi}_{\mathrm{e}}^{\mathrm{s}}$ are not determined uniquely. Thus, we can estimate whether the contact is f–f contact, and we can determine the direction of faces but not where the faces would be if the contact was f–f contact.

B. e–f and f–e contact estimation

A line and a plane intersect at a point. The point where the object edge line and the plane of the environmental face is given by

$$\boldsymbol{P}^{\mathrm{b}} = \begin{bmatrix} \boldsymbol{n}_{\mathrm{e}}^{\mathrm{b}} \times \boldsymbol{m}_{\mathrm{o}}^{\mathrm{b}} + h_{\mathrm{e}}^{\mathrm{b}} \boldsymbol{d}_{\mathrm{o}}^{\mathrm{b}} \\ \boldsymbol{n}_{\mathrm{e}}^{\mathrm{b}} \cdot \boldsymbol{d}_{\mathrm{o}}^{\mathrm{b}} \end{bmatrix} \tag{9}$$

If the contact between the object and the surroundings is an e–f contact, the edge line lies on the plane. The singular geometrical condition for the intersection is the case when Eq. (9) is a zero vector. Thus, we can define the objective function for e–f contact as follows:

$$\begin{aligned} F_{\mathrm{ef}} = \sum_{i=1}^{k} \Big(& \left\| (\boldsymbol{R}_i \boldsymbol{n}_{\mathrm{e}}^{\mathrm{s}}) \times \boldsymbol{m}_{\mathrm{o}}^{\mathrm{b}} + ((\boldsymbol{R}_i \boldsymbol{n}_{\mathrm{e}}^{\mathrm{s}}) \cdot \boldsymbol{p}_i + h_{\mathrm{e}}^{\mathrm{s}})\, \boldsymbol{d}_{\mathrm{o}}^{\mathrm{b}} \right\|^2 \\ & + \left\| (\boldsymbol{R}_i \boldsymbol{n}_{\mathrm{e}}^{\mathrm{s}}) \cdot \boldsymbol{d}_{\mathrm{o}}^{\mathrm{b}} \right\|^2 \Big). \end{aligned} \tag{10}$$

By transforming Eq. (10) to remove $\boldsymbol{L}_{\mathrm{o}}^{\mathrm{b}}$ and $\boldsymbol{\Pi}_{\mathrm{e}}^{\mathrm{s}}$ from the summation, we obtain

$$\begin{aligned} F_{\mathrm{ef}} = & \left(\boldsymbol{L}_{\mathrm{o}}^{\mathrm{b}} \otimes \boldsymbol{\Pi}_{\mathrm{e}}^{\mathrm{s}}\right)^{\mathrm{T}} \left(\sum_{i=1}^{k} \boldsymbol{A}_{\mathrm{ef}i}^{\mathrm{T}} \boldsymbol{A}_{\mathrm{ef}i} \right) \left(\boldsymbol{L}_{\mathrm{o}}^{\mathrm{b}} \otimes \boldsymbol{\Pi}_{\mathrm{e}}^{\mathrm{s}}\right) \\ & + \left(\boldsymbol{d}_{\mathrm{o}}^{\mathrm{b}} \otimes \boldsymbol{n}_{\mathrm{e}}^{\mathrm{s}}\right)^{\mathrm{T}} \left(\sum_{i=1}^{k} \mathrm{vec}\left(\boldsymbol{R}_i^{\mathrm{T}}\right) \mathrm{vec}\left(\boldsymbol{R}_i^{\mathrm{T}}\right)^{\mathrm{T}} \right) \left(\boldsymbol{d}_{\mathrm{o}}^{\mathrm{b}} \otimes \boldsymbol{n}_{\mathrm{e}}^{\mathrm{s}}\right), \end{aligned} \tag{11}$$

where

$$\boldsymbol{A}_{\mathrm{ef}i} = \begin{bmatrix} -\boldsymbol{p}_i^{\mathrm{sbT}} & 1 & \boldsymbol{0}^{\mathrm{T}} & 0 & \boldsymbol{0}^{\mathrm{T}} & 0 & & 0 \\ \boldsymbol{0}^{\mathrm{T}} & 0 & -\boldsymbol{p}_i^{\mathrm{sbT}} & 1 & \boldsymbol{0}^{\mathrm{T}} & 0 & \boldsymbol{B}_{\mathrm{ef}i} & 0 \\ \boldsymbol{0}^{\mathrm{T}} & 0 & \boldsymbol{0}^{\mathrm{T}} & 0 & -\boldsymbol{p}_i^{\mathrm{sbT}} & 1 & & 0 \end{bmatrix}. \tag{12}$$

and

$$\boldsymbol{B}_{\mathrm{ef}i} = \begin{bmatrix} \boldsymbol{0}^{\mathrm{T}} & 0 & \boldsymbol{r}_{3i}^{\mathrm{T}} & 0 & -\boldsymbol{r}_{2i}^{\mathrm{T}} & 0 \\ -\boldsymbol{r}_{3i}^{\mathrm{T}} & 0 & \boldsymbol{0}^{\mathrm{T}} & 0 & \boldsymbol{r}_{1i}^{\mathrm{T}} & 0 \\ \boldsymbol{r}_{2i}^{\mathrm{T}} & 0 & -\boldsymbol{r}_{1i}^{\mathrm{T}} & 0 & \boldsymbol{0}^{\mathrm{T}} & 0 \end{bmatrix}. \tag{13}$$

If the object moves under the constraint of e–f contact, Eq. (11) has a small value, and $\boldsymbol{L}_{\mathrm{o}}^{\mathrm{b}}$ and $\boldsymbol{\Pi}_{\mathrm{e}}^{\mathrm{s}}$ that makes Eq. (11) are the object edge and the environmental face in the e–f contact,respectively.

The objective function for f–e contact F_{fe} can be obtained by exchanging the spatial frame and the object frame. Here we omit the details because the derivation is the same as above, but F_{fe} is the function of $\boldsymbol{\Pi}_{\mathrm{o}}^{\mathrm{b}}$ and $\boldsymbol{L}_{\mathrm{e}}^{\mathrm{s}}$.

C. v–f and f–v contact estimation

A point and a plane span the entire space of a 3D space. In a four-dimensional(4D) space, which is the homogeneous space of the 3D space, the space spanned by the point and the plane has a volume. The volume of the point of the object vertex and the plane of the environmental face is given by

$$\boldsymbol{V} = \boldsymbol{q}_{\mathrm{o}}^{\mathrm{b}} \cdot \boldsymbol{n}_{\mathrm{e}}^{\mathrm{b}} - \alpha_{\mathrm{o}}^{\mathrm{b}} h_{\mathrm{e}}^{\mathrm{b}}. \tag{14}$$

If the vertex is on the environmental face, the scalar value of volume becomes zero. Thus, we can define the objective function for v–f contact by

$$F_{\mathrm{vf}} = \sum_{i=1}^{k} \left\| \boldsymbol{q}_{\mathrm{o}}^{\mathrm{b}} \cdot (\boldsymbol{R}_i \boldsymbol{n}_{\mathrm{e}}^{\mathrm{s}}) - \alpha_{\mathrm{o}}^{\mathrm{b}} \left((\boldsymbol{R}_i \boldsymbol{n}_{\mathrm{e}}^{\mathrm{s}}) \cdot \boldsymbol{p}_i - h_{\mathrm{e}}^{\mathrm{s}} \right) \right\|^2. \tag{15}$$

In the same manner as with other contact cases, by transforming Eq. (15) to make the target variables outside of the summation, we get

$$F_{\mathrm{vf}} = \left(\boldsymbol{P}_{\mathrm{o}}^{\mathrm{b}} \otimes \boldsymbol{\Pi}_{\mathrm{e}}^{\mathrm{s}}\right)^{\mathrm{T}} \left(\sum_{i=1}^{k} \boldsymbol{a}_{\mathrm{vf}i} \boldsymbol{a}_{\mathrm{vf}i}^{\mathrm{T}}\right) \left(\boldsymbol{P}_{\mathrm{o}}^{\mathrm{b}} \otimes \boldsymbol{\Pi}_{\mathrm{e}}^{\mathrm{s}}\right), \quad (16)$$

where

$$\boldsymbol{a}_{\mathrm{vf}i} = \begin{bmatrix} \begin{bmatrix} \boldsymbol{r}_{1i} \\ 0 \end{bmatrix}^{\mathrm{T}} & \begin{bmatrix} \boldsymbol{r}_{2i} \\ 0 \end{bmatrix}^{\mathrm{T}} & \begin{bmatrix} \boldsymbol{r}_{3i} \\ 0 \end{bmatrix}^{\mathrm{T}} & - \begin{bmatrix} \boldsymbol{c}_{1i} \cdot \boldsymbol{p}_i \\ \boldsymbol{c}_{2i} \cdot \boldsymbol{p}_i \\ \boldsymbol{c}_{3i} \cdot \boldsymbol{p}_i \\ 1 \end{bmatrix}^{\mathrm{T}} \end{bmatrix}^{\mathrm{T}}. \quad (17)$$

In the above matrix,$\boldsymbol{c}_1$, $\boldsymbol{c}_2$, and $\boldsymbol{c}_3$ are the first, second, and third column of $\boldsymbol{R}$, respectively.

The objective function for f–v contact F_{fv} is also obtained by exchanging the spatial frame and the object frame as the function of $\boldsymbol{\Pi}_{\mathrm{o}}^{\mathrm{b}}$ and $\boldsymbol{P}_{\mathrm{e}}^{\mathrm{s}}$.

D. e–e contact estimation

The same as with a point and a plane, two lines span the space in the 4D space. The following equation provides the volume of the space spanned by the object and environmental edge:

$$\boldsymbol{V} = \boldsymbol{d}_{\mathrm{o}}^{\mathrm{b}} \cdot \boldsymbol{m}_{\mathrm{e}}^{\mathrm{b}} + \boldsymbol{m}_{\mathrm{o}}^{\mathrm{b}} \cdot \boldsymbol{d}_{\mathrm{e}}^{\mathrm{b}}. \quad (18)$$

Thus, the objective function is its singular condition

$$F_{\mathrm{ee}} = \sum_{i=1}^{k} \left\| \boldsymbol{d}_{\mathrm{o}}^{\mathrm{b}} \cdot (\boldsymbol{R}_i \boldsymbol{m}_{\mathrm{e}}^{\mathrm{s}} - (\boldsymbol{R}_i \boldsymbol{d}_{\mathrm{e}}^{\mathrm{s}}) \times \boldsymbol{p}_i) + \boldsymbol{m}_{\mathrm{o}}^{\mathrm{b}} \cdot (\boldsymbol{R}_i \boldsymbol{d}_{\mathrm{e}}^{\mathrm{s}}) \right\|^2. \quad (19)$$

By transforming Eq. (19), the followings are given:

$$F_{\mathrm{ee}} = \left(\boldsymbol{L}_{\mathrm{e}}^{\mathrm{s}} \otimes \boldsymbol{L}_{\mathrm{o}}^{\mathrm{b}}\right)^{\mathrm{T}} \left(\sum_{i=1}^{k} \boldsymbol{a}_{\mathrm{ee}i} \boldsymbol{a}_{\mathrm{ee}i}^{\mathrm{T}}\right) \left(\boldsymbol{L}_{\mathrm{e}}^{\mathrm{s}} \otimes \boldsymbol{L}_{\mathrm{o}}^{\mathrm{b}}\right), \quad (20)$$

where

$$\boldsymbol{a}_{\mathrm{ee}i} = \begin{bmatrix} \begin{bmatrix} \boldsymbol{p}_i \times \boldsymbol{r}_{1i} \\ \boldsymbol{r}_{1i} \end{bmatrix}^{\mathrm{T}} & \begin{bmatrix} \boldsymbol{r}_{1i} \\ \boldsymbol{0} \end{bmatrix}^{\mathrm{T}} \\ \begin{bmatrix} \boldsymbol{p}_i \times \boldsymbol{r}_{2i} \\ \boldsymbol{r}_{2i} \end{bmatrix}^{\mathrm{T}} & \begin{bmatrix} \boldsymbol{r}_{2i} \\ \boldsymbol{0} \end{bmatrix}^{\mathrm{T}} \\ \begin{bmatrix} \boldsymbol{p}_i \times \boldsymbol{r}_{3i} \\ \boldsymbol{r}_{3i} \end{bmatrix}^{\mathrm{T}} & \begin{bmatrix} \boldsymbol{r}_{3i} \\ \boldsymbol{0} \end{bmatrix}^{\mathrm{T}} \end{bmatrix}^{\mathrm{T}}. \quad (21)$$

E. PC identification

In the above sections, we derived the objective functions for the six kinds of PCs; f–f, e–f, f–e, v–f, f–v, and e–e–c. By minimizing these functions by changing the pose of geometries (point, line, or plane), we can determine the contact geometry in each PC cases. The objective functions are also used to identify which PC the contact is for the measured motion of an object. When we minimize the objective function of a PC for the object's motion under the constraint of another PC, the resulting value of the function may be larger than the case in which we minimize it for the correct PC. Thus, it is possible to identify the PC by optimizing the geometries by the objective functions for a certain period of the object's motion and by comparing the minimization results. Even in the case when the object moved with the change in the PCs, we can identify them by setting the time window, shifting it, and applying the above comparison. We show this via by the experiments described in the following section.

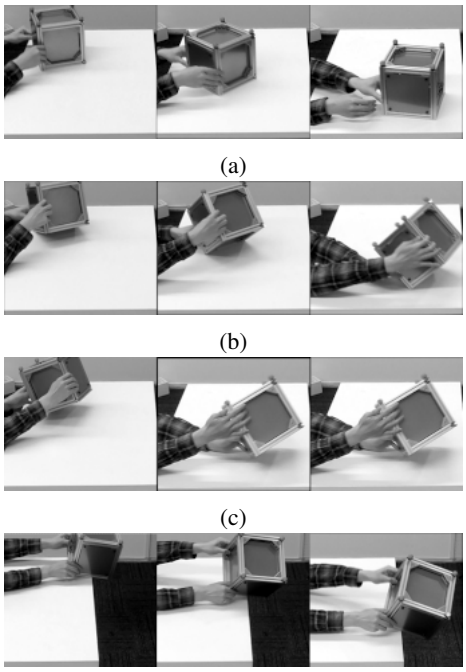

(a) (b) (c) (d)

Fig. 2: Four kinds of motion when we moved the object in the first experiment; (a) f–f, (b) f–e or e–f (c) f–v or v–f, and (d) e–e–c.

IV. Experiments

A. Method

We derived the objective functions to estimate the PCs based on the positions and orientation above. In this section, we describe the experiments used to validate the proposed functions with the data of the motion of an object moved in contact with the environment as measured by a motion capture system.

In the experiment, a person moved an object while making contact with the environment (a desk), as shown in Fig. 2. The object was a cube made of aluminum frames and stainless steel plates, as shown in Fig. 3. The size was $0.2\,\mathrm{m}^2$ and weighed $2.84\,\mathrm{kg}$. Four markers for the optical motion capture system were attached to the top of the object. The motion capture system specified the rigid body motion of the object from the marker positions. The motion capture system was a Kestrel Digital Real Time System (Motion Analysis Co., Santa Rosa, CA, USA), and the measurements were performed at $200\,\mathrm{Hz}$.

We conducted two kinds of experiments. In the first experiment, we estimated the geometries of contact for the motion constrained by the specified PC using the proposed objective functions for f–f, e–f, e–v, and e–e contact independently,

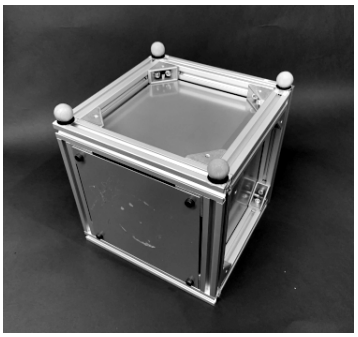

Fig. 3: Cube used in the experiment.

and compared the estimated and actual geometries. In the second experiment, we moved the object by changing the contacts (f–f, e–f, e–v, and e–e contact) for specific periods. We applied the objective functions to the data to compare the minimum values to identify the PC using the difference.

In the first experiment, first, we moved the object manually to maintain the PCs one by one and measured the motion. We excluded the data that shows the stationary object before the contact estimation because the measurement of the motion capture began before moving the object. By using the rest of the data, we optimized the corresponding objective functions via the sequential least squares programming (SQSLP) method for the demonstrated PC and estimated the PC geometries. The optimization was performed using ten different random initial values to avoid optimization failure owing to its local minima.

The second experiment was performed as follows: We moved the object after waiting $5\,\mathrm{s}$ after the motion measurement began. Then we demonstrated each contact for $10\,\mathrm{s}$ in the following order, f–f, e–f, e–v, and e–e contact. For each contact, the object was moved randomly, and it took various positions and orientations. We picked up 500 frames of data from the obtained data by moving the time window by ten frames from first to last. We minimized the objective functions of four PCs (f–f, e–f, e–v, and e–e contact) in each data set obtained from the time window using the SQSLP method. The optimization was performed with three different initial values to prevent failure. We compared the transition of the minimum values obtained by different objective functions. In the next section, we describe how the values of the objective functions were rescaled by the maximum value for ease of comparison.

B. Result

The results for the estimation of the geometries are shown in Fig. 4. Figure 4a shows the estimated normal of the faces (the red arrow for the object's face and the blue arrow for the environmental face) for f–f contact. Both for the object and the environment, the difference in angle between the correct face and the estimated face was $0.12°$. The location of the faces shifted from the bottom of the cube, as mentioned above. Figure 4b shows the estimated edge of the object (red line) and the environmental face's normal (blue arrow) for

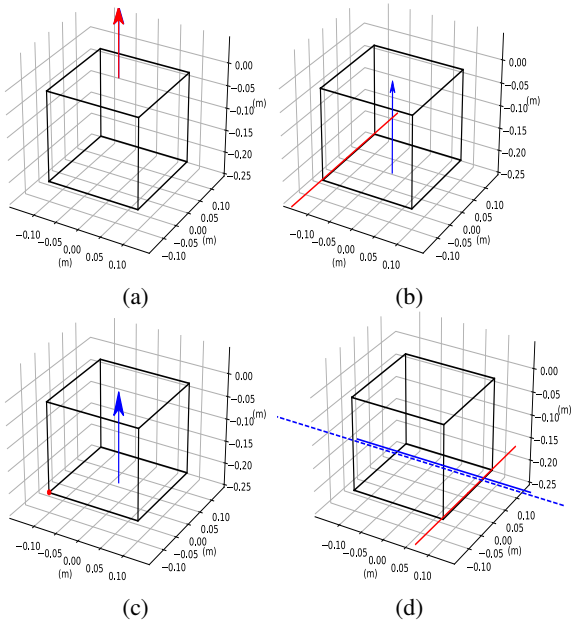

Fig. 4: Results of the contact geometry estimation for (a) f–f, (b) f–e or e–f (c) f–v or v–f, and (d) e–e–c.

e–f contact. The difference in distance and angle between the correct object edge and the estimated object edge was $0.0056\,\mathrm{m}$ and $0.76°$ respectively. The difference in angle between the correct environmental face and the estimated environmental face was $0.72°$. Figure 4c shows the estimated vertex of the object (red point) and the environmental face's normal (blue arrow) for v–f contact. The difference in distance between the correct object vertex and the estimated object vertex was $0.0094\,\mathrm{m}$. The difference in angle between the correct environmental face and the estimated environmental face was $0.14°$. Finally, figure 4d shows the estimated edge of the object (red line), the correct edge of the environment (blue dashed line), and the estimated edge of the environment(blue line). The difference in distance and angle between the correct object edge and the estimated object edge was $0.0063\,\mathrm{m}$ and $0.43°$ respectively. The difference in distance and angle between the correct environmental edge and the estimated environmental edge was $0.0040\,\mathrm{m}$ and $0.15°$ respectively.

The result for the transition of contact is shown in Fig. 5. The transition of the contact is shown as dotted vertical lines in the graph. The values for each function are normalized to a maximum value of 1 in the graph. The objective function for f–f and e–f contact kept taking small values during its target contact, and starts to take larger values for other contacts. The objective function for v–f contact also seems to work well overall, where as some failures were observed in the v–f contact phase (near the window of 530). We expected the the objective function for e–e contact, to retain low values during f–f, e–f, and e–e contact, and take higher values for v–f contact. However the difference in the values seemed small between e–e and v–f contact. We discuss the details of this result in the next section.

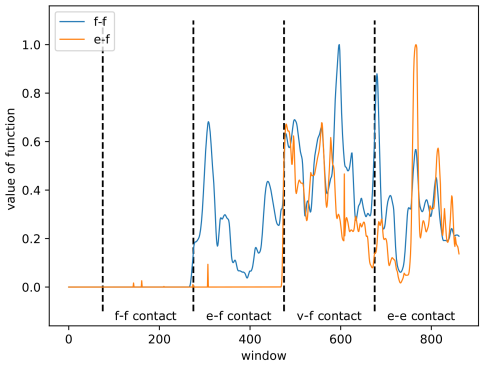

(a)

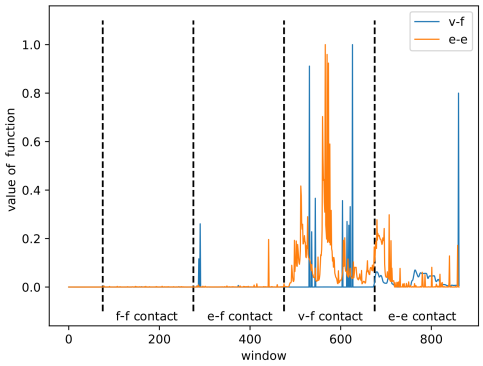

(b)

Fig. 5: Transition of minimum values of the objective functions. (a) Cases of f–f and e–f contact and (b) cases of v–f and e–e contact.

V. Conclusion

In this study, we derived the objective functions for the estimation of PCs for f–f, e–f, f–e, v–f, f–v, and e–e contact. We showed that the minimization of the derived functions correctly estimated the geometries of the contact for e–f, v–f, e–e, although there was a theoretical limitation to identify the location ofthe faces during f–f contact. A standard optimization algorithm could efficiently solve the minimization of the functions expressed by differential quadratic forms of the Kronecker product of homogeneous representation of the geometry. Thus, we can determine where the contact is for any kind of PC except for f–f contact (we can only see the direction of the normal), even if we have no idea of the geometry of the target object or its surroundings. In this study we only dealt with the case of a CF with a single PC. In the case of a CF containing several of the same PCs, the objective functions have several solutions, and it will appear as a local minima. In the case in which a CF contains several different PCs, the corresponding objective functions provide independent solutions and geometries. As a result, estimation of the PCs' geometry in a CF requires some optimization to determine every local minima.

In the second experiment, we minimized different objective functions at the same time for parts of the data divided by a time window during the changing sequence of motion in the PCs. The comparison between the minimum values of different functions implies the possibility that the proposed objective functions are available for identification of the type of PC in the manipulation. It is trivial that the geometrical constraint on the object motion generated by some PCs contains the geometrical constraint of other PCs. For example, the geometrical constraint for e–f contact is satisfied by the geometrical constraint for f–f contact. The result shows the containment relationship. An f–f contains an e–f, a v–f, and an e–e, and an e–f contains a v–f and an e–e, as the corresponding objective functions also resulted in small values for the contained contact. Thus, the identification of PCs in the motion with a change in PCs requires a prediction model that takes into account all the objective functions comprehensively.

The objective functions proposed here are the initial step to realizing the estimation of the CF between unknown objects during complicated compliant manipulation. There are problems that need to be solved, such as the classification of a specified motion. We cannot distinguish the contact from the motion, as mentioned in Section II. The measurement noise will also be a problem for realizing a stable estimation. The introduction of the probabilistic model and the measurement of the difference of applied force depending on the CFs will achieve stable estimation, and they are our future studies. Additionally, the values of the objective functions depend on how the object is moved. Future experiments are needed to evaluate the robustness of our method.

References

[1] T. Lefebvre, J. Xiao, H. Bruyninckx, and G. De Gersem, "Active compliant motion: a survey," *Adv. Robot.*, vol. 19, no. 5, pp. 479–499, 2005.

[2] R. S. Desai and R. A. Volz, "Identification and verification of termination conditions in fine motion in presence of sensor errors and geometric uncertainties," in *Proc. IEEE Int. Conf. Robot. Autom.*, 1989, pp. 800–807.

[3] J. K. Salisbury, "Interpretation of contact geometries from force measurements," in *Proc. IEEE Int. Conf. Robot. Autom.*, 1984, pp. 240–247.

[4] Y. Fei and X. Zhao, "An assembly process modeling and analysis for robotic multiple peg-in-hole," *J. Intell. Robot. Syst.*, vol. 36, no. 2, pp. 175–189, 2003.

[5] T. Lefebvre, H. Bruyninckx, and J. De Schutter, "Exact non-linear Bayesian parameter estimation for autonomous compliant motion," *Adv. Robot.*, vol. 18, no. 8, pp. 787–799, 2004.

[6] K. Gadeyne, T. Lefebvre, and H. Bruyninckx, "Bayesian hybrid model-state estimation applied to simultaneous contact formation recognition and geometrical parameter estimation," *Int. J. Robot. Res.*, vol. 24, no. 8, pp. 615–630, 2005.

[7] W. Meeussen, J. Rutgeerts, K. Gadeyne, H. Bruyninckx, and J. De Schutter, "Contact-state segmentation using particle filters for programming by human demonstration in compliant-motion tasks," *IEEE Trans. Robot.*, vol. 23, no. 2, pp. 218–231, 2007.

[8] S. Cabras, M. E. Castellanos, and E. Staffetti, "Contact-state classification in human-demonstrated robot compliant motion tasks using the boosting algorithm," *IEEE Trans. Syst., Man, Cybern. B. Cybern.*, vol. 40, no. 5, pp. 1372–1386, 2010.

[9] I. F. Jasim and P. W. Plapper, "T-S fuzzy contact state recognition for compliant motion robotic tasks using gravitational search-based clustering algorithm," in *Proc. IEEE Int. Conf. on Fuzzy Syst.*, 2013, pp. 1–8.

[10] K. Hertkorn, M. A. Roa, C. Preusche, C. Borst, and G. Hirzinger, "Identification of contact formations: Resolving ambiguous force torque information," in *Proc. IEEE Int. Conf. Robot. Autom.*, 2012, pp. 3278–3284.
[11] T. J. Debus, P. E. Dupont, and R. D. Howe, "Contact state estimation using multiple model estimation and hidden Markov models," *Int. J. Robot. Res.*, vol. 23, no. 4-5, pp. 399–413, 2004.
[12] N. Mimura and Y. Funahashi, "Parameter identification of contact conditions by active force sensing," in *Proc. IEEE Int. Conf. Robot. Autom.*, 1994, pp. 2645–2650.
[13] T. Mouri, T. Yamada, Y. Funahashi, and N. Mimura, "Identification of contact conditions from contaminated data of contact moment," in *Proc. IEEE Int. Conf. Robot. Autom.*, vol. 1, 1999, pp. 585–591.
[14] T. Mouri, T. Yamada, A. Iwai, N. Mimura, and Y. Funahashi, "Identification of contact conditions from position and velocity information," in *Proc. IEEE/RSJ Int. Conf. Intell. Robots Syst*, vol. 1, 2003, pp. 523–528.
[15] M. Mason, *Mechanics of robotic manipulation*. MIT press, 1985.
[16] J. Xiao, "Automatic determination of topological contacts in the presence of sensing uncertainties," in *Proc. IEEE Int. Conf. Robot. Autom.*, 1993, pp. 65–70.
[17] J. Xiao and X. Ji, "Automatic generation of high-level contact state space," *Int. J. Robot. Res.*, vol. 20, no. 7, pp. 584–606, 2001.
[18] N. L. White, "Grassmann–Cayley algebra and robotics applications," in *Handbook of Geometric Computing*. Springer, 2005, pp. 629–656.
[19] L. Dorst, D. Fontijne, and S. Mann, *Geometric algebra for computer science: an object-oriented approach to geometry*. Elsevier, 2010.